NANO LETTERS

LETTER

pubs.acs.org/NanoLett

Superfast-Response and Ultrahigh-Power-Density Electromechanical Actuators Based on Hierarchal Carbon Nanotube Electrodes and Chitosan

Jinzhu Li,[†,⊥,#] Wenjun Ma,[‡,#] Li Song,[§] Zhiqiang Niu,[†] Le Cai,[†,⊥] Qingsheng Zeng,[∥] Xiaoxian Zhang,[∥] Haibo Dong,[†,⊥] Duan Zhao,[†,⊥] Weiya Zhou,[†] and Sishen Xie*[,†]

[†]Beijing National Laboratory for Condensed Matter, Institute of Physics, Chinese Academy of Sciences, Beijing 100190, China

[‡]Faculty for Physics, Ludwig-Maximilians University of Munich (LMU), Am Coulombwall 1, D-85748 Garching, Germany

[§]Research Center for Exotic Nanocarbons, Shinshu University, Nagano City 380-8553, Japan

[∥]Key Laboratory for the Physics and Chemistry of Nanodevices, Department of Electronics, Peking University, Beijing 100871, China

[⊥]Graduate School of the Chinese Academy of Sciences, Beijing 100049, China

Supporting Information

ABSTRACT: Here we report a novel single-walled carbon nanotube (SWNT) based bimorph electromechanical actuator, which consists of unique as-grown SWNT films as double electrode layers separated by a chitosan electrolyte layer consisting of an ionic liquid. By taking advantage of the special hierarchical structure and the outstanding electrical and mechanical properties of the SWNT film electrodes, our actuators show orders-of-magnitude improvements in many aspects compared to previous ionic electroactive polymer (i-EAP) actuators, including superfast response (19 ms), quite wide available frequency range (dozens to hundreds of Hz), incredible large stress generating rate (1080 MPa/s), and ultrahigh mechanical output power density (244 W/kg). These remarkable achievements together with their facile fabrication, low driving voltage, flexibility, and long durability enable the SWNT-based actuators many applications such as artificial muscles for biomimetic flying insects or robots and flexible deployable reflectors.

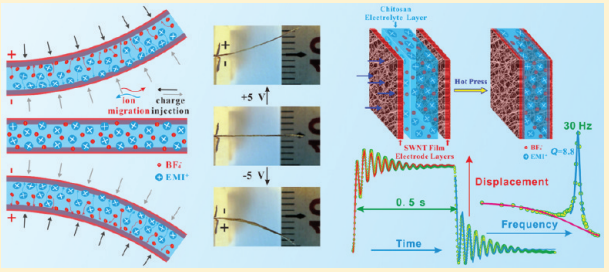

KEYWORDS: Electromechanical actuators, carbon nanotube, chitosan, resonant enhancement, superfast response, ultrahigh power density

Electromechanical actuator materials that directly convert electrical energy to mechanical energy have great potential for many applications including artificial muscles for robots and biomimetic flying, optical switches and microsensors, and so on.[1−5] In the last few decades, electromechanical actuators based on carbon nanotubes (CNTs),[2,6−8] conductive polymers,[9,10] dielectric elastomers,[11] ferroelectric polymers,[12−14] and graphene[5,15] have been successfully realized. Among these electroactive materials, dielectric elastomers and ferroelectric polymers have shown large strain, fast response, and strong electromechanical coupling, but they usually require high driving voltages (typically >1 kV) and high activation fields (∼150 MV/m) which limit their application in some cases.[3,11,12] Recently, ionic electroactive polymer (i-EAP) actuators have attracted increasing attention due to their lightweight, low driving voltage, and operability without aqueous solution.[3,4] However, the slow response (time scale of seconds to minutes), very low and narrow available frequency range (usually <1 Hz), and insufficient mechanical output abilities severely discourage their development and potential applications.[4]

CNTs have shown high specific surface area and exceptional mechanical and electrical properties, making them prime candidates for high strength composites[16−18] and energy storage and conversion devices.[19−21] Recent research showed that by introducing CNTs into the electrode layers, some electromechanical performances like respond speed and strain (stress) generating rate of i-EAP actuators could be improved.[22,23] For instance, Hata and co-workers have reported second-generation dry i-EAPs actuators using supergrowth single-walled carbon nanotubes (SG-SWNTs) as electrodes. Superb mechanical and electrical properties of the SG-SWNTs sheets give their actuators much faster strain and stress rates (2.28%/s and 3.26 MPa/s, respectively).[22] However, fabrication of i-EAP actuators with superfast response and ultrahigh mechanical output abilities still remain a great challenge because of the lack of perfect electrode material and efficient synthesis method.

In this paper, we demonstrate a facile way to fabricate a novel SWNTs-based bimorph i-EAP actuator. Instead of using dispersed CNTs as additives in the electrodes, we employed free-standing SWNT films with hierarchal structure and superior

Received: June 24, 2011
Revised: September 6, 2011
Published: October 05, 2011

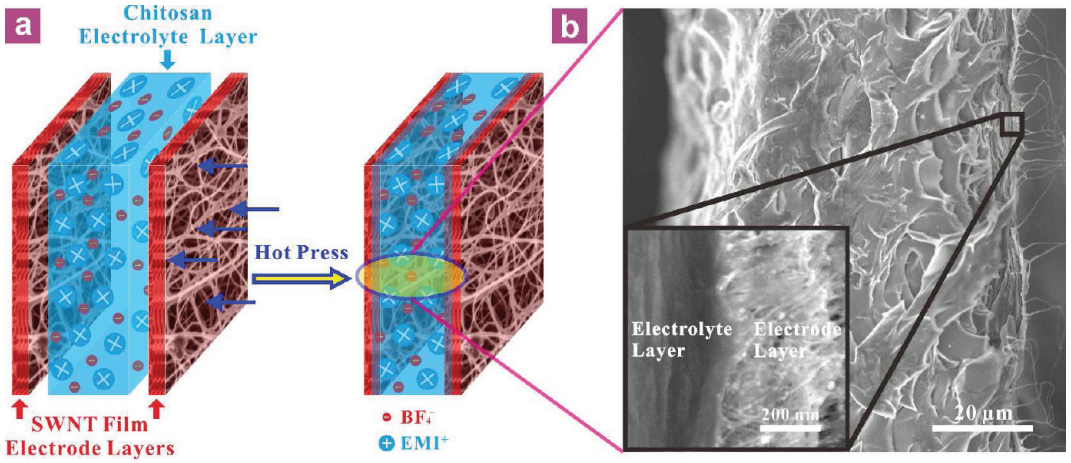

Figure 1. Assembly and structural characterization of the SWNTs-based actuators. (a) Schematic diagram of the assembly and bimorph configuration of an actuator. (b) Typical SEM cross-sectional image of a bimorph configured actuator. Inset: the enlarged image of a selected zone of the boundary.

mechanical and electrical properties as electrodes. Such SWNT films are directly synthesized by floating catalyst chemical vapor deposition (FCCVD), in which SWNTs are strongly bonded as a hierarchal network during their growth at high temperature. Long (micrometer scale) and strong interbundle shear-legs give this SWNT film high electrical conductivity (2000 s/cm), modulus (5 GPa), and strength (360 MPa).[24−26] As shown in Figure 1a, the SWNTs-based actuator was constructed by sandwiching a half-dried chitosan/ion liquid electrolyte layer with two pieces of as-grown free-standing SWNT films as electrode layers via a facile and effective hot-press process (for more experimental detail see S1 in the Supporting Information). The biocompatible polymer chitosan and an ion liquid $EMIBF_4$ are chosen here because they not only show good compatibility with CNTs but also are promising candidates as supporting polymer and mobile ion donor for electrolyte layers of i-EAP electrochemical actuators.[27−30] With such sandwich structure and hot-press process, our actuators can benefit much from the unique SWNT films. First, porous hierarchical structure of the SWNT films and good compatibility among all components permit good interlayer adhesions between the electrode layers and the middle electrolyte layer (Figure 1b), which are very crucial for any high-performance electromechanical actuators. Second, superior electrical conductivity of the SWNT films guarantees the extremely small surface resistance of the electrode layers (10 Ω/□), resulting in a very small voltage drop along the actuator surface and making the whole actuator a parallel-plate capacitor.[31,32] Combined with the high specific surface of CNTs, charge injection and ion migration between electrodes are greatly facilitated, which give rise to a large and fast bending displacement response of the actuators. Third, owing to the outstanding mechanical properties of the SWNT films, both modulus and strength of the actuators are effectively enhanced.[33] With the well-bonded hierarchical SWNT networks as skeletons, the electrode layers have a Young's modulus about 12−14 GPa and the average modulus for the whole actuator is about 1−2 GPa, which are significantly higher than that of the electrolyte layer (400 MPa) and the actuators with dispersed CNTs based composites as electrode layers (200 MPa).[22] The average strength of the actuator is 50 MPa, which is also much higher than normal polymers and soft actuators based on them. These

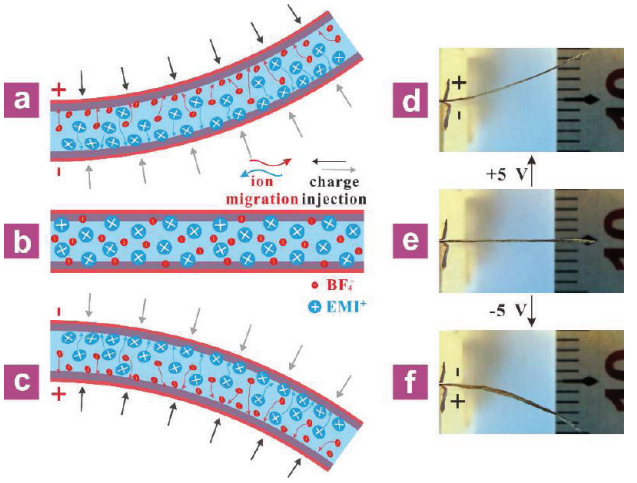

Figure 2. Electromechanical actuation mechanism of the SWNTs-based actuator. (a−c) Actuation illustration of the bimorph configured actuator under positive (a), negative (c), and no (b) extra electrical field. (d−f) The corresponding photographs of an actuator with a positive (d), negative (f), and no (e) applied voltage of 5 V, well confirm the electromechanical actuation mechanism.

highly improved mechanical properties of the actuators essentially lead to high mechanical output work and power densities.

Similar to previous reports, our electromechanical actuators are expected to be charge injection and ion migration dominated rather than Faradaically driven.[2,22] A conceivable electromechanical actuation mechanism is illustrated in panels a−c of Figure 2, when an electrical field is applied between the two electrode layers, steric effects induced by electrochemical charge injection (double layer charging) and subsequent ion migration and accumulation provide the expansion of cathode and the contraction of anode, which result in bending displacements toward the anode.[2,22,29,30] Panels d−f of Figures 2 show the corresponding photographs of a typical SWNTs-based actuator with and without an applied voltage of 5 V. The observed fast and large displacements well confirm the electromechanical actuation mechanism. Comparing to previous ionic polymer/metal composites (IPMCs) like Pt−Nafion actuators that work in electrolyte solutions, actuations in these i-EAPs actuators require no

dx.doi.org/10.1021/nl202132m |Nano Lett. 2011, 11, 4636–4641

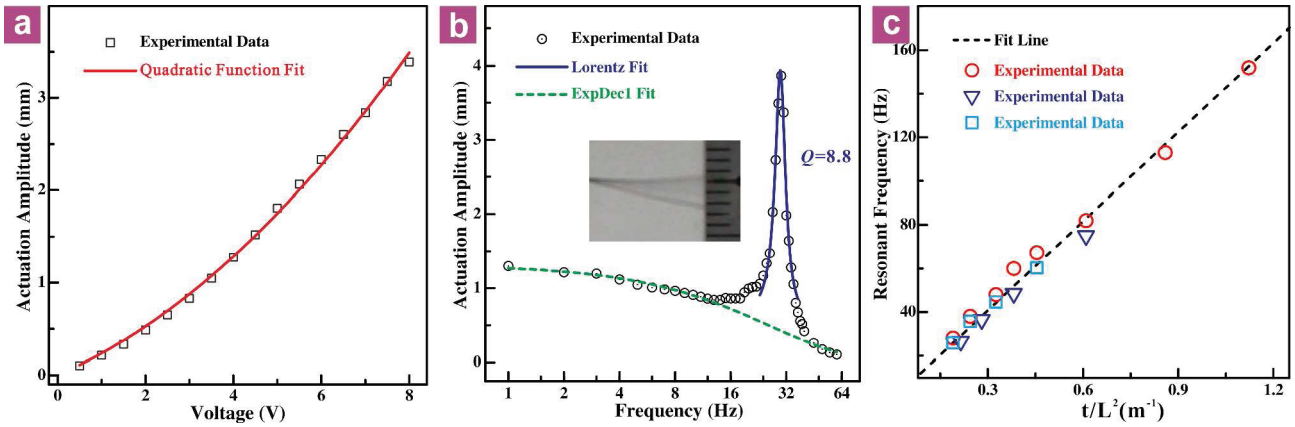

Figure 3. Electromechanical actuation performances of the SWNT-based actuator. (a) Actuation amplitude (maximum displacement) of an actuator under different square wave voltages with frequency of 1 Hz. Open squares represent the experimental data, and the red solid line shows a quadratic function fitting. (b) Actuation amplitude for an actuator with a resonant enhancement around 30 Hz under a ±4 V square wave potential with respect to the driving frequency ranging from 1 to 60 Hz. Black open circles are the experimental data, a green dashed line is the best fitting line for the data away from the resonance zone using the first order exponential decay (ExpDec1) function, and the blue solid line represents the resonance peak fitting to a Lorentzian line shape with a quality factor Q = 8.8. The inset is an optical image of the actuator flapping at the resonant frequency of 30 Hz with amplitude about 4 mm. (c) Geometry-dependent fundamental resonant frequencies for actuators scaling to t/L^2, which is well consistent with the beam theory. The dashed line gives the expected value using $(Y/\rho)^{1/2}$ = 850 m/s.

participation of water molecules; thus they do not have the drawback of relaxation behaviors induced by back diffusion of water.[34] When triangle wave voltages of 1 Hz are applied to the actuator, the displacement−voltage curves show that the displacement is proportional to the voltage and the displacement loops exhibit little hysteresis even at higher voltages (see S2 in the Supporting Information), indicating the fast response of these devices.

Figure 3a shows that when square wave voltages with a given frequency are applied, the actuation amplitude (maximum displacement) of the SWNT-based actuator quadratically increases with the applied potential, indicating that the displacement amplitude can be well controlled by changing the voltages. The actuation amplitude, stress (strain) generating rate, and work (power) density for the actuator with respect to the driving frequency are shown in Figures 3b, 4a, and 4b, respectively (calculation for related performance parameters see S1 in the Supporting Information). As the frequency increases from 1 to 60 Hz, the actuation amplitude performs exponential decay along with a prominent peak gain at about 30 Hz, which is assigned to the resonant frequency of the cantilever-type actuator. At the resonant frequency, the actuator provides astonishingly high mechanical output capabilities. The maximum strain generating rate is up to 9%/s. To our knowledge, this strain rate is the highest value achieved in i-EAPs,[22,30] although still not comparable with the strain rate achieved in dielectric elastomers which have a much faster electrostatic actuation mechanism.[3,11] The derived stress generating rate is as high as 1080 MPa/s, which is much higher than the peak capability of natural and other artificial muscles (30 MPa/s).[3] Furthermore, the maximum output work density is 2.03 J/kg, and the maximum power density is 244 W/kg, which also far exceeds the peak capability of human skeletal muscles (50 W/kg) and approaches the highest value attained in animals (284 W/kg).[3]

It is common sense that the output capabilities of cantilever-type actuators could be greatly amplified if they work at their resonant frequencies. Nanomechanical resonators based on single CNTs or their bundles working at their resonant frequencies have already been successfully utilized for ultrasensitive mass measurement and force detection.[35−37] However, such resonant enhancements were seldom realized for macroscale actuators at a resonant frequency higher than 10 Hz,[2,7] the working frequency for many important applications such as biomimetic flying. For most macroscale electromechanical i-EAPs actuators, the resonant enhancements of their actuation amplitudes are not obvious because of the limitation from their charge injection and ion migration rates. As a result of inadequate charging, the actuation amplitudes decrease dramatically as the frequency increases, thus the resonant enhancements are restricted to very low levels, which depress their potential for applications at high frequency. In the case of our actuators, hierarchal SWNT electrodes permit much faster charge injection and ion migration rates and result in the large actuation amplitude and output abilities at resonant frequency as we see.

To prove this, we excite the actuator with a square wave potential. As shown in Figure 5a, its normalized displacement versus time curve at 1 Hz expresses nearly square waveform with a small-amplitude damping vibration. Steep rising (falling) edges of the displacement indicate the fast actuation response of the actuator, which can be seen more clearly from the enlarged extracted period (Figure 5b). Following the initial steep rising (falling), there are multipeaks which exhibit perfect sinusoidal waveform with damped amplitude. We assign this unique damping vibration to the instant actuating force excited by the fast actuation response, which arises from the rapid charge injection and ion migration in the actuator. The whole bending process (up and down) can be described using a model which combines a time-dependent charging (discharging) model with a sinusoidal damping model. Here we name it the electromechanical damping (EMD) model, in which the time-dependent displacement can be expressed by following function (derivation details and analyses for 2 and 5 Hz, see S3 and S4 in the Supporting Information)

$$\delta(t) = \delta_0(1 - e^{-t/\tau}) + A_0 e^{-\beta t} \sin[2\pi f_d(t + t_c)] \qquad (1)$$

where τ represents the electromechanical actuation response

dx.doi.org/10.1021/nl202132m |Nano Lett. 2011, 11, 4636–4641

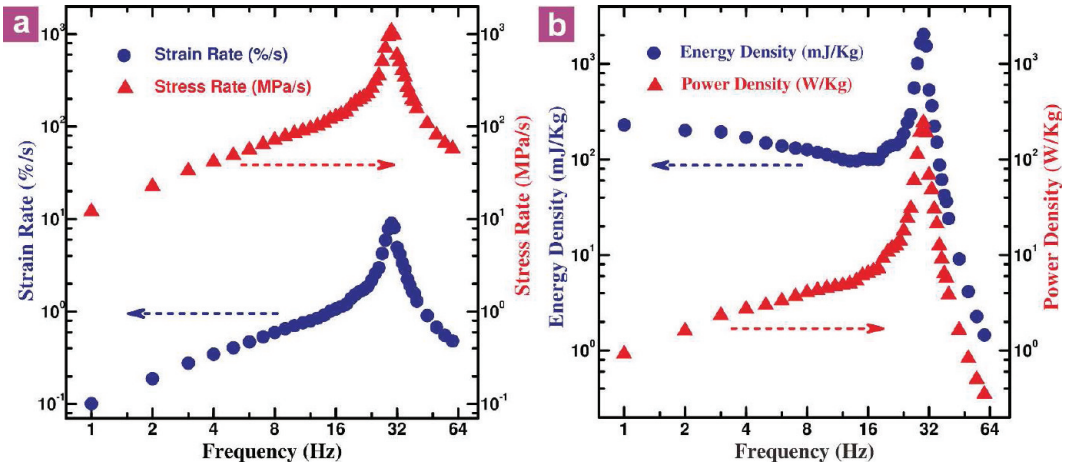

Figure 4. High mechanical output abilities of the SWNTs-based actuator. Strain and stress generating rates in the electrode layers (a) as well as the corresponding mechanical output work and power densities (b) as a function of the driving frequency.

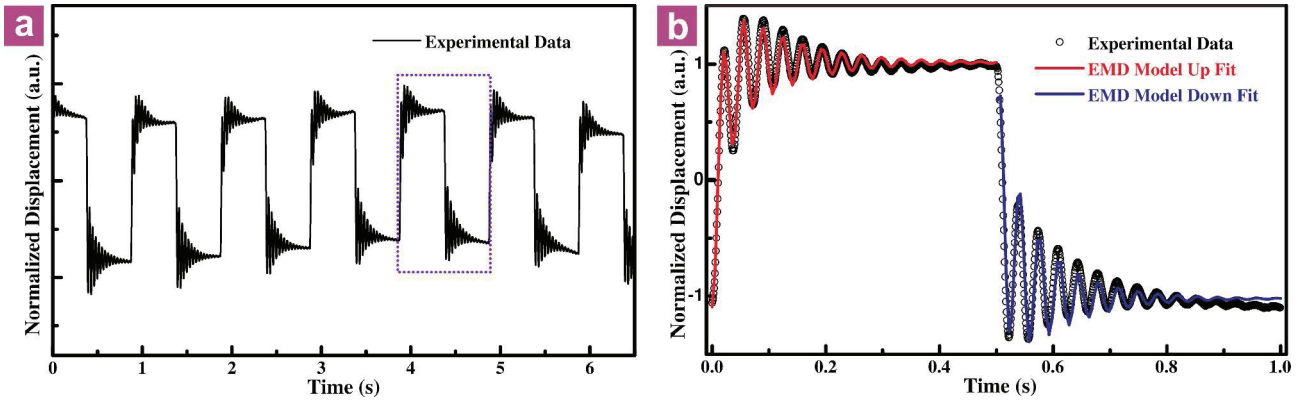

Figure 5. Superfast electromechanical actuation response of the SWNTs-based actuator. (a) Normalized displacement versus time under ±4 V square wave voltage of 1 Hz. (b) One period extracted from (a) for model analysis. Black open circles represent the experimental data while the red and blue solid lines are the best fitting lines using the EMD model (eq 1).

time constant and β and f_d are the exponential decay rate and damped natural frequency of the cantilever-type actuator, respectively. A smaller τ means a faster electromechanical bending response, implying faster rates of charge injection and ion migration. From Figure 5b, we can see that both the fitting lines for up and down bending processes using the EMD model (eq 1) match the experimental data very well. The fitting value for the response time τ is as low as 19 ms, which is much faster than the typical response time scale of seconds to minutes for traditional i-EAP actuators, and comparable with the response time scale of milliseconds for electromagnetic actuators, piezoceramics, and natural muscles.[3,4]

With this superfast response time, the unique amplitude-frequency curve for our actuator can be better understood. As shown in Figure 3b, the green dashed line gives the best fitting result for the data away from the resonance zone using the first-order exponential decay function (ExpDec1), and a corresponding frequency bandwidth as high as 18 Hz is obtained. It indicates that with the increase of frequency up to 18 Hz, the decrease of the raw actuation amplitude (without consideration of the resonant enhancement) is still less than 50%. Even to the high frequency of 30 Hz, the raw actuation amplitude is still larger than $^1/_3$ of that at 1 Hz. Therefore, comparing with previous slow response i-EAPs actuators, the actuation amplitude of our actuators gains more effective resonant enhancement (triple the value at 1 Hz). Lorentzian fitting for the resonance peak gives a mechanical quality factor Q of 8.8 for our actuator devices (Figure 3b). Compared with the typical Q factor (40−200) for the nanomechanical resonators,[35−37] this value is quite low. But considering the vibration mechanism (ion displacement inside the polymer), the ambient air pressure and temperature, and the macroscale dimension (centimeter length) of our devices, this Q value is reasonable. Because of the resonant enhancement, the frequency bandwidth extends to 37 Hz (with amplitude decrease less than 50%). This unexpected slow actuation amplitude decay makes this actuator a promising energy convert device that can work in a wide frequency range, such as slower bending displacements for artificial limbs at low frequency and faster flapping vibrations for biomimetic flying insects or robots at high frequency.

According to the beam theory, the geometry-dependent fundamental resonant frequency of the singly clamped cantilever-type actuator can be given by[36]

$$f_R = 0.16 \frac{t}{L^2}\sqrt{\frac{Y}{\rho}} \qquad (2)$$

dx.doi.org/10.1021/nl202132m |Nano Lett. 2011, 11, 4636–4641

where t, L, Y, and ρ are the thickness, free length, average Young's modulus, and mass density of the cantilever-type actuator, respectively. Figure 3c shows the measured resonant frequencies for actuators scaling to t/L^2. Fits to the measured data using eq 2 with specific modulus as free parameter show good agreement with the experimental data. Therefore, by changing the geometry of the actuator, its resonant frequency can be easily tuned in a quite wide range from dozens to hundreds of Hz, which fits the wing-beat-frequency of most flying insects, for example, ~10 Hz for a butterfly, ~40 Hz for a dragonfly, and ~200 Hz for a housefly. In particular, via shaping the actuator like a wing and matching its resonant frequency with the wing-beat-frequency of insects, a biomimetic flying insect or robot may eventually be successfully designed in the future. Here we give a demonstrated video for an actuator flapping at resonant frequency of 30 Hz with magnitude about 4 mm (S5 in the Supporting Information).

For actuators working at resonant frequency, their durability may be an issue. We also would like to mention that our actuators have long durability besides their incredible large stress generating rate and high output power density. Bending measurements indicate that under ±5 V square wave potential at resonant frequency of 30 Hz, the actuation amplitude has no obvious decline within more than 6000 running circles. SEM images of the actuator surfaces show there are no observable electrode damages after the electromechanical actuation. This long durability can be attributed to the unique flexibility of SWNTs as well as the compact and robust structure of the actuators. For the cantilever actuators shown in this paper, mechanical/mass loading will decrease their resonant frequency and displacement amplitude, thus their work and power densities. In future studies, their actuation performances under mechanical load need to be investigated for biomimetic applications.

In summary, we demonstrate a novel bimorph configured electromechanical actuator based on SWNT films, biocompatible polymer chitosan, and an ionic liquid. Full exploitation of the special hierarchal structure and the outstanding electrical and mechanical properties of the as-grown SWNT film electrodes facilitate the highly improved performances of the actuator, including superfast response (19 ms), quite wide available frequency range (dozens to hundreds of hertz), incredible large stress generating rate (1080 MPa/s), and ultrahigh output power density (244 W/kg). Furthermore, we established an EMD model to evaluate the fast response of our actuator, which provides excellent agreement with the experimental data, gives better understanding of the electromechanical actuation mechanism, and also can be extended to simulate other damping behaviors in mechanical systems based on kinds of different mechanisms.

Considering of these remarkable achievements together with their facile fabrication, lightweight, flexibility, long durability, biocompatibility, low driving potential (several voltages), and controllability in air (without aqueous solution), we believe the SWNT-based actuators shown here will have great potential for various applications, such as artificial muscles for biomimetic flying insects or robots and flexible deployable reflectors and so on.

■ ASSOCIATED CONTENT

Ⓢ Supporting Information. Experimental details, displacement−voltage curves under a triangle wave potential, derivation of the electromechanical damping (EMD) model (eq 1), fast response analyses for 2 and 5 Hz with the EMD model, and a video for an actuator flapping at resonant frequency of 30 Hz with magnitude about 4 mm. This material is available free of charge via the Internet at http://pubs.acs.org.

■ AUTHOR INFORMATION

Corresponding Author

*E-mail: ssxie@aphy.iphy.ac.cn.

Author Contributions

#These authors contributed equally to this work.

■ ACKNOWLEDGMENT

We thank Keyence, Y. Gao, L. Liu, and Z. Zhang for assistance with bending and mechanical tests and helpful discussion. This work was supported by the National Basic Research Program of China (Grant No. 2012CB932302), the National Natural Science foundation of China (Grant No. 90921012, 51172271), Beijing Municipal Education Commission (Grant No. YB20108000101), and the Key Item of Knowledge Innovation Project of Chinese Academy of Sciences (KJCX2-YW-M01). L. Song was supported by Exotic Nanocarbons, Japan Regional Innovation Strategy Program by Excellence, JST, and the Green Innovation Project from Shinshu University.

■ REFERENCES

(1) Shahinpoor, M.; Bar-Cohen, Y.; Simpson, J. O.; Smith, J. *Smart Mater. Struct.* **1998**, *7*, R15–R30.

(2) Baughman, R. H.; Cui, C. X.; Zakhidov, A. A.; Iqbal, Z.; Barisci, J. N.; Spinks, G. M.; Wallace, G. G.; Mazzoldi, A.; De Rossi, D.; Rinzler, A. G.; Jaschinski, O.; Roth, S.; Kertesz, M. *Science* **1999**, *284*, 1340–1344.

(3) Madden, J. D. W.; Vandesteeg, N. A.; Anquetil, P. A.; Madden, P. G. A.; Takshi, A.; Pytel, R. Z.; Lafontaine, S. R.; Wieringa, P. A.; Hunter, I. W. *IEEE J. Oceanic Eng.* **2004**, *29*, 706–728.

(4) *Electroactive Polymer (EAP) Actuators as Artificial Muscles: Reality, Potential and Challenges*; Bar-Cohen, Y., Ed.; SPIE Press: Bellingham, WA, 2004.

(5) Zhu, S. E.; Shabani, R.; Rho, J.; Kim, Y.; Hong, B. H.; Ahn, J. H.; Cho, H. J. *Nano Lett.* **2011**, *11*, 977–981.

(6) Fennimore, A. M.; Yuzvinsky, T. D.; Han, W. Q.; Fuhrer, M. S.; Cumings, J.; Zettl, A. *Nature* **2003**, *424*, 408–410.

(7) Aliev, A. E.; Oh, J. Y.; Kozlov, M. E.; Kuznetsov, A. A.; Fang, S. L.; Fonseca, A. F.; Ovalle, R.; Lima, M. D.; Haque, M. H.; Gartstein, Y. N.; Zhang, M.; Zakhidov, A. A.; Baughman, R. H. *Science* **2009**, *323*, 1575–1578.

(8) Chen, L. Z.; Liu, C. H.; Liu, K.; Meng, C. Z.; Hu, C. H.; Wang, J. P.; Fan, S. S. *ACS Nano* **2011**, *5*, 1588–1593.

(9) Baughman, R. H. *Synth. Met.* **1996**, *78*, 339–353.

(10) Lu, W.; Fadeev, A. G.; Qi, B. H.; Smela, E.; Mattes, B. R.; Ding, J.; Spinks, G. M.; Mazurkiewicz, J.; Zhou, D. Z.; Wallace, G. G.; MacFarlane, D. R.; Forsyth, S. A.; Forsyth, M. *Science* **2002**, *297*, 983–987.

(11) Pelrine, R.; Kornbluh, R.; Pei, Q. B.; Joseph, J. *Science* **2000**, *287*, 836–839.

(12) Zhang, Q. M.; Bharti, V.; Zhao, X. *Science* **1998**, *280*, 2101–2104.

(13) Zhang, Q. M.; Li, H. F.; Poh, M.; Xia, F.; Cheng, Z. Y.; Xu, H. S.; Huang, C. *Nature* **2002**, *419*, 284–287.

(14) Lehmann, W.; Skupin, H.; Tolksdorf, C.; Gebhard, E.; Zentel, R.; Kruger, P.; Losche, M.; Kremer, F. *Nature* **2001**, *410*, 447–450.

(15) Xie, X. J.; Qu, L. T.; Zhou, C.; Li, Y.; Zhu, J.; Bai, H.; Shi, G. Q.; Dai, L. M. *ACS Nano* **2010**, *4*, 6050–6054.

(16) Ajayan, P. M.; Tour, J. M. *Nature* **2007**, *447*, 1066–1068.
(17) Mamedov, A. A.; Kotov, N. A.; Prato, M.; Guldi, D. M.; Wicksted, J. P.; Hirsch, A. *Nat. Mater.* **2002**, *1*, 190–194.
(18) Coleman, J. N.; Khan, U.; Blau, W. J.; Gun'ko, Y. K. *Carbon* **2006**, *44*, 1624–1652.
(19) An, K. H.; Kim, W. S.; Park, Y. S.; Moon, J. M.; Bae, D. J.; Lim, S. C.; Lee, Y. S.; Lee, Y. H. *Adv. Funct. Mater.* **2001**, *11*, 387–392.
(20) Pushparaj, V. L.; Shaijumon, M. M.; Kumar, A.; Murugesan, S.; Ci, L.; Vajtai, R.; Linhardt, R. J.; Nalamasu, O.; Ajayan, P. M. *Proc. Natl. Acad. Sci. U.S.A.* **2007**, *104*, 13574–13577.
(21) Meng, C. Z.; Liu, C. H.; Chen, L. Z.; Hu, C. H.; Fan, S. S. *Nano Lett.* **2010**, *10*, 4025–4031.
(22) Mukai, K.; Asaka, K.; Sugino, T.; Kiyohora, K.; Takeuchi, I.; Terasawo, N.; Futoba, D. N.; Hata, K.; Fukushima, T.; Aida, T. *Adv. Mater.* **2009**, *21*, 1582–1585.
(23) Liu, S.; Liu, Y.; Cebeci, H.; de Villoria, R. G.; Lin, J. H.; Wardle, B. L.; Zhang, Q. M. *Adv. Funct. Mater.* **2010**, *20*, 3266–3271.
(24) Song, L.; Ci, L.; Lv, L.; Zhou, Z. P.; Yan, X. Q.; Liu, D. F.; Yuan, H. J.; Gao, Y.; Wang, J. X.; Liu, L. F.; Zhao, X. W.; Zhang, Z. X.; Dou, X. Y.; Zhou, W. Y.; Wang, G.; Wang, C. Y.; Xie, S. S. *Adv. Mater.* **2004**, *16*, 1529–1532.
(25) Ma, W. J.; Song, L.; Yang, R.; Zhang, T. H.; Zhao, Y. C.; Sun, L. F.; Ren, Y.; Liu, D. F.; Liu, L. F.; Shen, J.; Zhang, Z. X.; Xiang, Y. J.; Zhou, W. Y.; Xie, S. S. *Nano Lett.* **2007**, *7*, 2307–2311.
(26) Ma, W. J.; Liu, L. Q.; Zhang, Z.; Yang, R.; Liu, G.; Zhang, T. H.; An, X. F.; Yi, X. S.; Ren, Y.; Niu, Z. Q.; Li, J. Z.; Dong, H. B.; Zhou, W. Y.; Ajayan, P. M.; Xie, S. S. *Nano Lett.* **2009**, *9*, 2855–2861.
(27) Fukushima, T.; Kosaka, A.; Ishimura, Y.; Yamamoto, T.; Takigawa, T.; Ishii, N.; Aida, T. *Science* **2003**, *300*, 2072–2074.
(28) Liu, Y.; Wang, M. K.; Zhao, F.; Xu, Z. A.; Dong, S. J. *Biosens. Bioelectron.* **2005**, *21*, 984–988.
(29) Fukushima, T.; Aida, T. *Chem.—Eur. J.* **2007**, *13*, 5048–5058.
(30) Lu, L. H.; Chen, W. *Adv. Mater.* **2010**, *22*, 3745–3748.
(31) Cui, Y.; Kaempgen, M.; Chan, C. K.; Ma, J.; Gruner, G. *Nano Lett.* **2009**, *9*, 1872–1876.
(32) Niu, Z. Q.; Zhou, W. Y.; Chen, J.; Feng, G. X.; Li, H.; Ma, W. J.; Li, J. Z.; Dong, H. B.; Ren, Y.; Zhao, D. A.; Xie, S. S. *Energ. Environ. Sci.* **2011**, *4*, 1440–1446.
(33) Li, J. Z.; Gao, Y.; Ma, W. J.; Liu, L. Q.; Zhang, Z.; Niu, Z. Q.; Ren, Y.; Zhang, X. X.; Zeng, Q. S.; Dong, H. B.; Zhao, D.; Cai, L.; Zhou, W. Y.; Xie, S. S. *Nanoscale* **2011**, *3*, 3731–3736.
(34) Nemat-Nasser, S.; Wu, Y. X. *J. Appl. Phys.* **2003**, *93*, 5255–5267.
(35) Sazonova, V.; Yaish, Y.; Ustunel, H.; Roundy, D.; Arias, T. A.; McEuen, P. L. *Nature* **2004**, *431*, 284–287.
(36) Jensen, K.; Kim, K.; Zettl, A. *Nat. Nanotechnol.* **2008**, *3*, 533–537.
(37) Chiu, H. Y.; Hung, P.; Postma, H. W. C.; Bockrath, M. *Nano Lett.* **2008**, *8*, 4342–4346.